C. R. Physique 16 (2015) 628–640

Contents lists available at ScienceDirect

Comptes Rendus Physique

www.sciencedirect.com

Gamma-ray astronomy / Astronomie des rayons gamma

# On the origin of very-high-energy photons in astrophysics: A short introduction to acceleration and radiation physics

## *De l'origine des photons de très haute énergie en astrophysique : une brève introduction aux mécanismes d'accélération et de rayonnement*

Martin Lemoine [a,*], Guy Pelletier [b]

[a] *Institut d'astrophysique de Paris, CNRS–UPMC, 98 bis, boulevard Arago, 75014 Paris, France*
[b] *Institut de planétologie et d'astrophysique de Grenoble, UJF–Université Grenoble-1/CNRS–INSU, 34, rue de la Piscine, 38000 Grenoble, France*

ARTICLE INFO

*Article history:*
Available online 1 October 2015

*Keywords:*
Particle acceleration
Cosmic rays
Gamma-rays
High-energy astrophysics

*Mots-clés :*
Accélération de particules
Rayons cosmiques
Photons gamma
Astrophysique des hautes énergies

ABSTRACT

Powerful astrophysical sources produce non-thermal spectra of very-high-energy photons, with generic power-law distributions, through various radiative processes of charged particles, e.g., synchrotron radiation, inverse Compton processes, and hadronic interactions. Those charged particles have themselves been accelerated to ultra-relativistic energies in intense electromagnetic fields in the source. In many cases, the exact acceleration scheme is not known, but standard scenarios, such as Fermi mechanisms and reconnection processes are generally considered as prime suspects for the conversion of bulk kinetic or electromagnetic energy into a power law of supra-thermal particles. This paper proposes a short introduction to the various acceleration and radiative processes which shape the distributions of very-high-energy photons ($\epsilon_\gamma \gtrsim 100$ MeV) in astrophysics.


RÉSUMÉ

Les sources astrophysiques puissantes sont à l'origine de spectres non thermiques de photons de très haute énergie, généralement caractérisés par des distributions en loi de puissance. Ces photons sont le fruit de processus radiatifs divers de particules chargées primaires, qui interagissent, par exemple, par rayonnement synchrotron, processus Compton inverse ou par des interactions hadroniques. Ces particules chargées ont, quant à elles, été accélérées à des énergies ultra-relativistes dans les champs électromagnétiques intenses des sources. Le mécanisme exact de l'accélération est bien souvent inconnu, mais les processus de Fermi, ou de reconnexion, sont généralement considérés comme des agents idéaux d'une conversion d'énergie d'ensemble, cinétique ou électromagnétique, en énergie de particules supra-thermiques. Cet article propose une brève introduction à la physique de ces processus d'accélération et de rayonnement, à la source des spectres de photons de très haute énergie ($\epsilon_\gamma \gtrsim 100$ MeV) en astrophysique.


* Corresponding author.
*E-mail addresses:* lemoine@iap.fr (M. Lemoine), guy.pelletier@obs.ujf-grenoble.fr (G. Pelletier).

http://dx.doi.org/10.1016/j.crhy.2015.08.012
1631-0705/

## 1. Introduction

The pioneering detections of high-energy photons from cosmic sources in the seventies have opened a whole new way of studying the Universe, through the non-thermal radiation produced by the most violent particle accelerators. One understands those manifestations through an apparently simple universal scheme: powerful sources accelerate charged particles in intense electromagnetic fields, and those particles then radiate non-thermal electromagnetic radiations via various electrodynamical processes.

In the past decades, high-energy-photon astronomy has thus become an unvaluable tool to study the physics of acceleration and radiation in the core of powerful astrophysical sources. Thanks to the development of large collecting area and high resolution detectors [1,2], we have reached now a stage in which modellers and theorists alike strive to understand a wealth of high-energy data from various sources, such as active galactic nuclei, compact objects, gamma-ray bursts, and supernovae.

However, as the devil lies in the details, an in-depth description of the non-thermal radiation of a source involves highly complex phenomena acting on different scales, combining hydrodynamics, relativity, electrodynamics, plasma physics in extreme conditions, and even particle physics at large. Accelerating particles in cosmic sources turns out to be a complex task, mostly because the high conductivity of astrophysical plasmas screens efficiently any electric field in the rest frame of the plasma. The physics of particle acceleration in astrophysical sources has thus become a field of study it its own right.

In contrast, radiation physics is well known, but accurate calculations of the emitted spectra are often fraught with approximations made in the description of the source on scales that are not accessible to observation. Characteristic examples include the detailed description of magnetized turbulence, which determine the synchrotron spectra, or that of radiative backgrounds with which the accelerated particles interact. A careful comparison of a model to the data thus requires to bridge, in one way or another, the gap between the microphysical scales of acceleration and radiation and the macrophysical scales of the source. These source models are discussed in the subsequent articles, while the present paper proposes a short introduction to the physics of acceleration and radiation inside high energy astrophysical sources.

General features of acceleration processes are discussed first (Section 2) and radiative processes next (Section 3). Section 4 provides a summary of the notions introduced with some perspectives. Two warnings are in order. One should first of all make a distinction between microphysical acceleration processes and bulk plasma acceleration mechanisms such as jet and wind launching: the acceleration processes that we are interested in give a possibly large fraction of the available energy to a minority of the plasma constituents, e.g., a power-law distribution in Lorentz factor $\gamma$, $\mathrm{d}N/\mathrm{d}\gamma \propto \gamma^{-p}$ with index $p > 1$, while the latter accelerate the bulk of the plasma. Although fascinating by itself, the topic of bulk plasma acceleration is not discussed here. Furthermore, given the breadth of the topics discussed here, it is of course impossible to do justice to either of these; hence, emphasis has been put on the fundamental physical processes, on modern developments and on some applications in high-energy astrophysics. The subsequent articles offer multiple examples of applications of the various processes that are discussed in the following.

## 2. Acceleration mechanisms

There exist a number of reviews discussing the physics of particle acceleration in astrophysical sources, e.g., [3–9]. Particles can be accelerated in electromagnetic fields through the Lorentz force

$$\frac{\mathrm{d}\boldsymbol{p}}{\mathrm{d}t} = q\,(\boldsymbol{E} + \boldsymbol{v}\times\boldsymbol{B}) \tag{1}$$

This fundamental equation is rich in useful lessons: the transverse character of the magnetic Lorentz force implies that the magnetic field does not exert work on the particle, so that acceleration requires an electric field. However, in a rest frame $\mathcal{R}_\mathrm{b}$ in which the ions of the background plasma are at rest, i.e. no bulk velocity, electric fields are generally screened on a microphysical timescale due to the large mobility of the electrons, implying[1] $\boldsymbol{E}_{|\mathbf{b}} = 0$. In the laboratory frame, in which Eq. (1) is written, in which the plasma moves at velocity $\boldsymbol{v}_\mathbf{p}$, there exists a motional electric field, $\boldsymbol{E} = -\boldsymbol{v}_\mathbf{p}\times\boldsymbol{B}$, associated with the Lorentz transform of the magnetic field; note that $\boldsymbol{B}$ is written here in the laboratory frame, which explains why no bulk Lorentz factor appears in this transform.

Therefore, in order to accelerate the particle in a general astrophysical setting, where ideal magneto-hydrodynamics (MHD) conditions apply, one must exploit the motional electric fields. This tells us that the acceleration timescale, in this laboratory frame, is at most of the order

$$t_\mathrm{acc} \lesssim \left|\frac{1}{p}\frac{\mathrm{d}\boldsymbol{p}}{\mathrm{d}t}\right|^{-1} \sim \frac{t_\mathrm{g}}{\beta_p} \tag{2}$$

where $t_\mathrm{g} = p/(eB)$ denotes the gyration time of the accelerated particle in the magnetic field, and $\beta_p = v_p/c$. This upper limit saturates if motion along $\boldsymbol{E}$ is regular; however, the above $\boldsymbol{E}$ is transverse to $\boldsymbol{B}$ (see further below for the possibility of a parallel component $\boldsymbol{E}_\parallel$), therefore one also needs an agent, e.g., a force or scattering events, to push the particles

[1] Throughout this article, we use the index notation, e.g., $_{|\mathrm{b}}$, to indicate that the quantity is expressed in a given frame, here $\mathcal{R}_\mathrm{b}$.

across the magnetic field. Indeed, if $\boldsymbol{B}$ is rectilinear and no such force exists, the particles simply cross-drift in the moving electromagnetic field, corresponding to helical motion around $\boldsymbol{B}_{|\mathbf{b}}$ in the $\mathcal{R}_\mathrm{b}$ frame.

The nature of this force is a useful way to discriminate among various acceleration mechanisms. For instance, scattering in turbulent flows allows the particle to interact with the electromotive fields associated with the moving eddies; scattering back and forth across the shock wave allows the particle to benefit from the electric fields of the moving structures, while shock-drift acceleration takes place when the particle executes deformed Larmor orbits around the perpendicular (with respect to the shock normal) background magnetic field at a shock front. Such examples are discussed in some detail in the following.

It is important to note that in relativistic flows, the notion of an acceleration timescale becomes itself frame-dependent, therefore some care must be taken in the choice of the proper frame in which to discuss the physics.

One may also note that the above equation may be generalized to rotating systems, e.g., pulsar winds or black hole magnetospheres, in which an electromotive force is induced by the rotating magnetic field structure; in that case $\boldsymbol{E} = -(\boldsymbol{\Omega}\times\boldsymbol{r})\times\boldsymbol{B}$, where $\Omega$ denotes the angular rotation vector and $\boldsymbol{r}$ the particle position. A net potential then exists between the poles of the object and the equator at infinity, which may lead to acceleration. In such objects, however, the acceleration process leads to a bulk acceleration of the whole plasma, which will not be discussed here.

In principle, there may exist linear accelerators in astrophysical sources, in which there exists a component of $\boldsymbol{E}$ parallel to $\boldsymbol{B}$, or in which $E > B$. Obviously, such sources do not satisfy to ideal MHD conditions; reconnection flows, in which resistive effects destroy the magnetic field in the current sheet are one such prominent example of that class. They will be discussed in Section 2, where it will be shown, in particular, that an acceleration of the form of Eq. (2) can nevertheless be defined.

Other examples of non-ideal MHD accelerators are wakefield and ponderomotive forces; the former accelerates particles in an electrostatic field that has been created in the wake of some electromagnetic disturbance. It may play an important role in the physics of relativistic magnetized shock waves [10–12]. The latter accelerates the particle in the gradient of an electromagnetic field structure, with a force $\propto \nabla B^2$.

The exact shape of the particle distribution function can be obtained by solving a transport equation in momentum space, accounting for the energy gains and particle losses (or energy losses). In the absence of particle escape from the accelerator, one generally expects to observe an exponential-like distribution peaking at a maximum momentum, at which the acceleration, escape and radiative timescales become comparable, with a cut-off above, where escape or radiative losses dominate. In the presence of particle escape, it can be shown that the particles follow a power-law $\mathrm{d}N/\mathrm{d}\gamma \propto \gamma^{-p}$ due to the competition between energy gain and escape. The number of particles $N(>\gamma) \propto \gamma^{1-p}$ then scales with the probability of achieving a Lorentz factor $> \gamma$, which scales as $(1-p_\mathrm{esc})^n$, with $p_\mathrm{esc}$ the probability of escape at each energy gain event and $n$ the number of energy gain events. The latter is given by $n \simeq \ln(\gamma/\gamma_0)/\ln\left(1+\langle\Delta\gamma/\gamma\rangle\right)$, in terms of $\gamma_0$ the injection Lorentz factor and $\langle\Delta\gamma/\gamma\rangle$ the mean relative energy gain per event. The index $p$ of the power-law then reads [13]

$$p \simeq 1 - \frac{\ln(1-p_\mathrm{esc})}{\ln\left(1+\langle\Delta\gamma/\gamma\rangle\right)} \tag{3}$$

In the case of diffusive acceleration at strong shock waves, it directly leads to an index $p \simeq 2.0$, as shown later in Section 2.2.

The high-energy cut-off is of great importance, because its observation brings information on the acceleration efficiency and the radiative properties of the source. If one writes the acceleration timescale as $t_\mathrm{acc} \equiv \mathcal{A} t_\mathrm{g}$, with $\mathcal{A} \gtrsim 1/\beta_p$ following the above discussion, then at least, one needs to match $t_\mathrm{acc}$ with the synchrotron loss timescale $t_\mathrm{syn} = \frac{4}{3}\sigma_\mathrm{T} U_\mathrm{B} \gamma_\mathrm{e} m_\mathrm{e} c$ for electrons ($U_\mathrm{B}$ denoting the magnetic field energy density, $\sigma_\mathrm{T}$ the Thomson cross-section and $\gamma_\mathrm{e}$ the Lorentz factor of the electron). This gives rise to the radiation reaction limiting Lorentz factor $\gamma_\mathrm{max} = 1.17{\cdot}10^8\,\mathcal{A}^{-1/2}B_{-4}^{-1/2}$ (with $B_{-4} = B/10^{-4}$ T; unless otherwise specified, we use the notation $Q_x = Q/10^x$ with $Q$ expressed in SI units). To this maximal Lorentz factor of the accelerated electron corresponds a maximal synchrotron photon energy [14]

$$\epsilon_{\gamma,\mathrm{max}} \sim \mathcal{A}^{-1}\frac{m_\mathrm{e}c^2}{\alpha_\mathrm{em}} \sim 70\,\mathcal{A}^{-1}\ \mathrm{MeV} \tag{4}$$

in terms of $\alpha_\mathrm{em}$ the fine structure constant. This maximal energy is independent of the magnetic field strength, provided $t_\mathrm{acc}$ indeed scales linearly with $t_\mathrm{g}$. The above maximal synchrotron photon energy has been written in the laboratory frame, in which the acceleration and radiation processes have been described; in the observer frame, the energy may be affected by a Lorentz boost.

### 2.1. Turbulent acceleration

The original model of E. Fermi in 1949 [15] relied on the interaction of a particle with (sub-relativistic) moving magnetized centers. The physics of acceleration can be depicted in this case as a kinematic process, in which the particle gains or loses energy through an elastic scattering with a moving structure: if the particle has mass $m$ and momentum

$\boldsymbol{p}$ (energy $E_p$) and scatters to momentum $\boldsymbol{p'}$ (energy $E'_p$), while the magnetic cloud has mass $M \gg m$ and momentum $\boldsymbol{q} \ll Mc$ (energy $E_q$), then energy-momentum conservation implies

$$\frac{\Delta E_p}{E_p} \simeq \frac{(\boldsymbol{p'} - \boldsymbol{p}) \cdot \boldsymbol{q}}{M E_p} + \mathcal{O}\left(\frac{\Delta p^2}{q^2}\right) \tag{5}$$

for $\Delta E_p \equiv E'_p - E_p$, indicating that energy gain takes place in head-on collisions, while energy loss occurs in tail-on collisions. The above result can be obtained (and generalized) by a double Lorentz transformation, in which one switches from the laboratory to the rest frame $\mathcal{R}$ of the moving structure, where the particle suffers pitch angle deflection at constant energy in the limit $M \gg m$, then Lorentz transforming back to the laboratory frame. Defining the velocities $\beta_p = pc/E_p$ and $\beta_q = qc/E_q$,

$$E'_p = \gamma_q^2 \left(1 - \beta_p \beta_q \cos\theta\right)\left(1 + \beta_p \beta_q \cos\theta'_{|\mathcal{R}}\right) E_p \tag{6}$$

where $\theta$ (resp. $\theta'_{|\mathcal{R}}$) denotes the angle between $\boldsymbol{p}$ (resp. $\boldsymbol{p'}$) and $\boldsymbol{q}$; note also that $\theta'_{|\mathcal{R}}$ is defined here in the frame of the magnetic cloud, while $\theta$ is expressed in the laboratory frame. In the sub-relativistic limit, i.e. $\gamma_q \equiv \left(1 - \beta_q^2\right)^{-1/2} \sim 1$, one recovers the previous formula.

On average, energy gain takes place due to the fact that head-on encounters are more frequent than tail-on encounters for a moving particle in a medium with an isotropic distribution of cloud velocities. Weighting the energy gain by the collision frequency $\nu_{\rm coll} \propto \left|\boldsymbol{\beta_p} - \boldsymbol{\beta_q}\right|$, assuming that $\cos\theta$ and $\cos\theta'_{|\mathcal{R}}$ are random variables, one obtains the average energy gain, which leads to advection in momentum space

$$\left\langle \frac{\Delta E_p}{E_p} \right\rangle \simeq \frac{4}{3}\beta_q^2 + \mathcal{O}\left(\beta_q^4\right) \tag{7}$$

and the variance, which represents the diffusion term in momentum space,

$$\left\langle \frac{\Delta E_p^2}{E_p^2} \right\rangle - \left\langle \frac{\Delta E_p}{E_p} \right\rangle^2 \simeq \frac{2}{3}\beta_q^2 + \mathcal{O}\left(\beta_q^4\right) \tag{8}$$

The evolution of the particle distribution function can be described by a Fokker–Planck equation in the limit $\beta_q \ll 1$ (small energy gain), characterized by the above advection and diffusion terms. These terms are of second order in $\beta_q$, one power of $\beta_q$ resulting from the difference in collision probability between head-on and tail-on, the other from the energy gain (when energy gain occurs). As $\beta_q \to 1$, the notion of first or second order loses its significance as energy gains can become of order unity, see, e.g., [16]; one cannot write down a Fokker–Planck equation in this case, since each interaction leads to a substantial energy gain, see [9].

As is well-known, the typical velocity of interstellar clouds, $\beta_q \sim 10^{-4}$, implies an acceleration timescale $t_{\rm acc} = \lambda/\langle \Delta E_p/E_p \rangle \propto \lambda \beta_q^{-2}$ that is so large that acceleration of cosmic rays cannot take place in regards of cooling losses through ionization of the interstellar gas. Nevertheless, this Fermi mechanism represents the proto-typical acceleration mechanism of particles interacting with motional electric fields. It can actually be generalized to acceleration through the interaction with a magnetized turbulence: in a first approximation, one can substitute the wave phase velocity, e.g., $v_{\rm A}$, for $\beta_q c$, and the scattering length $\ell_{\rm scatt}$ for $\lambda$. To obtain a better approximation of the transport, one needs to write down the explicit Fokker–Planck terms, which are obtained in quasi-linear theory from the Vlasov equation of the particle distribution function (e.g., [8] and references therein).

### 2.2. The Fermi process at strong shock waves

The above Fermi process can also take place when the particle bounces on magnetized media back and forth across a shock front [3,4,13,17–19]. Then, the energy gain becomes systematic due to the converging nature of the flow across the shock. In order to see this, one needs to define and distinguish various reference frames; in the so-called shock frame, in which the shock surface is at rest, the unshocked plasma (also called the upstream) is inflowing into the shock, while the shocked plasma (called the downstream) is flowing away from the shock at a sub-sonic velocity. As made clear in Fig. 1, if the particle is returning from downstream to upstream, moving towards $+\boldsymbol{x}$, then, as seen in the downstream frame, the particle sees a magnetized turbulence which moves towards $-\boldsymbol{x}$, which will imply a head-on collision if the particle returns towards downstream after the scattering event; the same can be said by exchanging upstream and downstream, once the particle is residing upstream.

More formally, one can use Eq. (6) again, replacing $\beta_q$ with $\beta_{\rm rel}$, the relative velocity between the upstream and downstream media: consider a particle initially residing upstream of the shock, with energy $E_p$, crossing to enter downstream with an angle[2] $\pi/2 \leq \theta \leq \pi$; in this case, $\beta_{\rm rel} > 0$ denotes the relative velocity between downstream and upstream, it is

[2] Actually, the condition to return downstream is $-1 \leq \cos\theta \leq \beta_{\rm sh}$, where $\beta_{\rm sh}$ denotes the velocity of the shock relative to upstream.

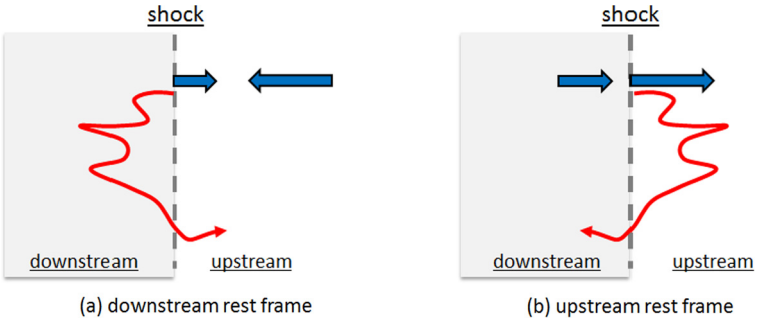


**Fig. 1.** (Colour online.) Sketch of the Fermi acceleration process as viewed in the downstream rest frame (a) and in the upstream rest frame (b). The arrows indicate the velocities of the shock front and of the upstream (a) [resp. downstream (b)] frame in the indicated rest frame.

oriented towards $+\boldsymbol{x}$ and therefore the term in the left brackets is positive; after having diffused downstream, the particle returns upstream with an angle[3] $0 \leq \theta' \leq \pi/2$, implying that the term in the right brackets is also positive. Independently of $\theta$ and $\theta'$, the energy gain is thus always positive. In the frame in which the shock is at rest, it is possible to show that the mean energy gain, obtained by weighing the energy gain for a single ultra-relativistic particle derived from the above equation with the flux and marginalizing over the random $\cos\theta$ and $\cos\theta'$ in the above intervals, is

$$\left\langle \frac{\Delta\gamma}{\gamma} \right\rangle \simeq \frac{4}{3}\beta_{\rm rel} \tag{9}$$

which is thus of first order in $\beta_{\rm rel}$; the above equation is valid in the sub-relativistic limit $\beta_{\rm rel} \ll 1$, see below for its generalization to relativistic flows. This acceleration mechanism is thus particularly efficient, and its application at the shock waves of supernova remnants is believed to explain the origin of cosmic rays with energy up to the so-called "knee" (which marks a break in the general power-law of the cosmic ray spectrum at an energy of $2{\cdot}10^{15}$ eV).

The competition between the energy gain, associated with the cycles of the particle around the shock front, and the possibility of escape from the acceleration site through advection with the downstream plasma,[4] leads to the emergence of a power law. The microphysical analysis of [13] shows that the escape probability at each cycle is $4\beta_{\rm sh}/r$, with $r = \beta_{\rm sh}/(\beta_{\rm sh} - \beta_{\rm rel})$ the shock compression ratio, while Eq. (9) gives the energy gain as $4(r-1)\beta_{\rm sh}/(3r)$. In accordance with the previous formula Eq. (3), the index is

$$p \simeq 1 + \frac{3}{r-1} \tag{10}$$

i.e., $p \simeq 2.0$ for a strong non-relativistic shock, for which $r = 4$. The consequences of Fermi-type acceleration at a supernova remnant shock front are discussed in this volume in [20].

In the above scheme, the particle distribution function gets isotropized through pitch angle diffusion in the magnetized turbulences on both sides of the shock front, hence this process is often referred to as "diffusive shock acceleration". Other mechanisms of acceleration are possible: for instance, if the particle interacts with a strong background magnetic field, it suffers "shock-drift acceleration", since the compression of the magnetic field at the shock front implies a drift along the motional electric field $\boldsymbol{E}$. Such acceleration is in general limited in extent, as the particle eventually escapes downstream (e.g., [5]).

No distinction is made here according to the obliquity of the magnetic field, although it is generally accepted that the physics of acceleration depends on the magnetic configuration. In particular, one should distinguish subluminal from superluminal shock waves [21]: in the former case, one can transform to a frame in which the magnetic field is aligned with the flow and the shock front is at rest, while in the latter no such transformation is possible, instead one can transform into a frame where the magnetic field is exactly perpendicular to the shock normal with the shock front at rest. Parallel shocks, with $\boldsymbol{B}$ oriented along the shock normal, thus belong to the former category, while perpendicular shocks belong to the latter. In parallel shock waves, particles can travel to arbitrarily large distances upstream and downstream of the shock front by circulating around the field lines, therefore diffusive shock acceleration is believed to operate according to the standard scheme. In a perpendicular configuration, however, particles must diffuse across the magnetic field lines in order to undergo diffusive shock acceleration, although shock-drift acceleration may be efficient in this case. At present, there is no general agreement on the efficiency of acceleration in either configuration, because this efficiency depends strongly on the type of turbulence which is excited on both sides of the shock front by the accelerated particles themselves; see [22,23] for recent simulations.

[3] As well, the exact condition is $\beta_{\rm sh|d} \leq \cos\theta' \leq 1$ so that the particle can outrun the shock, which is moving with velocity $\beta_{\rm sh|d}$ relative to downstream.

[4] In principle, escape does not occur upstream, since the upstream plasma is advected at the shock velocity towards the shock front, as viewed in the shock rest frame. However, the highest energy particles, which may explore the far upstream regions beyond the shock precursor, where the turbulence level is low, may decouple from the flow and escape upstream.

Most of the action today in this field of research is actually related to understanding the non-linear relationship between the physics of the collisionless shock, the acceleration of supra-thermal particles and the back-reaction of these particles on the magnetized turbulence in the immediate vicinity of the shock, see, e.g., [24] for analytical studies and [22,23] for numerical simulations. There are indeed evidence from multi-wavelength observations of supernova remnant shock waves that the magnetic field behind the shock front has been amplified to values one or two orders of magnitude larger than interstellar ones [25]. The leading mechanisms for this amplification are the streaming instability (e.g., [26]), its modern generalization (Bell instability [27]), according to which the net parallel current carried by the cosmic rays excite gyro-resonant or smaller scale modes in the background plasma, or a pressure driven instability [28].

Such an amplification is also warranted from a more phenomenological point of view, since it is well-known that at the Bohm limit, meaning $t_{\rm acc} = t_{\rm g}/\beta_{\rm sh}^2$, the maximum energy that protons can reach in supernovae remnant shocks falls short of the so-called knee of the cosmic ray spectrum by one or two orders of magnitude [29], whereas a stronger field could lead to enhanced confinement, hence a maximum energy closer to the so-called "knee" of the cosmic-ray spectrum. The maximum energy clearly has a direct impact on the production of gamma-rays, and the observation of $> 10$ TeV gamma-rays by Cherenkov telescopes certainly attests of the acceleration capabilities of these objects.

### 2.3. Acceleration at relativistic shock waves

As the shock velocity transits towards relativistic values, the physics of the acceleration become quite different. First and foremost, since the shock moves about as fast as the accelerated particle, diffusion does not have time to set-in on the upstream side of the trajectory. Actually, as viewed from the upstream rest frame, the particle is systematically caught back by the shock wave as soon as its velocity along the shock normal drops to values $\leq \beta_{\rm sh}$, i.e. as soon as it is deflected by an angle such that $\cos\theta \leq \beta_{\rm sh}$, or $\theta \sim 1/\Gamma_{\rm sh}$ [30,31]. Downstream, the particle must turn around quickly enough to catch back the shock front, which moves away at a large velocity, i.e. $\beta_{\rm sh|d} \simeq 1/3$ for a strong hydrodynamic shock solution. The energy gain also becomes substantial: it is of order $\langle \Delta\gamma/\gamma \rangle \sim \Gamma_{\rm sh}^2$ during the first Fermi cycle around the shock, although it drops to a factor $\sim$2 in subsequent cycles [31,32]. This latter result is not trivial; it directly stems from the anisotropy of the cosmic ray population upstream, focused within an angle $1/\Gamma_{\rm sh}$.

Furthermore, due to Lorentz transform effects, which boost the perpendicular (with respect to the shock normal) components of the magnetic field by $\Gamma_{\rm sh}$ while leaving unchanged the parallel component, when going from the upstream rest frame to the shock rest frame, relativistic shock waves are generically perpendicular (super-luminal) [33]. Unless scattering is strong behind the relativistic shock front, particles will thus be advected away with the magnetic field lines downstream of the shock front. Because the particles only probe a distance of the order of their gyroradius $r_{\rm g}$ behind the shock, before being reflected towards upstream or advected towards downstream, it is possible to show that only a small-scale turbulence, laid on scales $\lambda_{\delta B} \ll r_{\rm g}$ and of sufficiently intense strength $\delta B \gg (r_{\rm g}/\lambda) B_0$ ($B_0$ representing the background compressed field in the downstream frame), can unlock the particles from the field lines and allow the Fermi process to develop [34–37]. These conditions can be rewritten in terms of the background magnetisation of the flow, $\sigma = B_0^2/\left[\mu_0 \Gamma_{\rm sh}(\Gamma_{\rm sh}-1) n m_{\rm p} c^2\right]$, of the equipartition fraction of the magnetized turbulence $\epsilon_{\rm B} = \delta B^2/\left[\mu_0 \Gamma_{\rm sh}(\Gamma_{\rm sh}-1) n m_{\rm p} c^2\right]$ and in terms of the (downstream) plasma frequency as follows:

$$\sigma \lesssim \epsilon_{\rm B}^2 \left(\frac{\lambda_{\delta B}\omega_{\rm p}}{c}\right)^2 \tag{11}$$

for the supra-thermal particles of typical energy $\gamma_{\rm sh} m_{\rm p} c^2$; the former relation implies $\lambda_{\delta B} \lesssim c/\omega_{\rm p}$. Since a typical value of $\epsilon_{\rm B}$ is 0.01, this equation suggests that only weakly magnetized relativistic shock waves can accelerate particles efficiently [36,37]. This result has been confirmed by particle-in-cell (PIC) simulations, which indeed find an upper limit $\sigma \sim 10^{-4}$ for particle acceleration, in excellent qualitative agreement with the above [38]. The above relations also imply the existence of a maximum energy beyond which the Fermi process should no longer be operative, $E_{\rm max} \sim \gamma_{\rm sh} m_{\rm p} c^2 \epsilon_{\rm B}^2/\sigma$, since the efficiency of scattering in micro-turbulence decreases with increasing energy and beyond $E_{\rm max}$, the particles are advected away before being scattered.

The nature of the micro-turbulence is most likely related to the micro-instabilities that develop in the precursor of the relativistic shock through the interpenetration of the supra-thermal and background particle populations. At very low magnetization, the leading instability is the filamentation or Weibel instability [39]; as magnetization increases, a perpendicular current instability, triggered by the gyration of the supra-thermal particles in the background magnetic field, becomes dominant [40,41]. At even higher magnetizations $\sigma \gtrsim 0.1$, a synchrotron maser instability shapes the shock [10,11].

Much has been understood in the past decade or so in this field of research, but much also remains to be understood. In particular, how acceleration proceeds at magnetized, ultra-relativistic shock waves representative of the termination of pulsar winds remains a real challenge, see, e.g., [42] for a review, and also the contribution [20] in this volume. Although the above arguments suggest that the Fermi process should not take place, the reconstruction of the electron distribution in the Crab nebula and similar objects rather suggests a power-law with index $s = 2.2$, in excellent agreement with the predictions of the test particle simulations assuming isotropic scattering downstream of the shock (e.g., [31,32,43–45]). Another essential question is how acceleration proceeds in the mildly relativistic limit, $\gamma_{\rm sh}\beta_{\rm sh} \sim 1$ and, in particular, what are the leading plasma instabilities that shape the magnetized turbulence in that region of parameter space, see [46] for

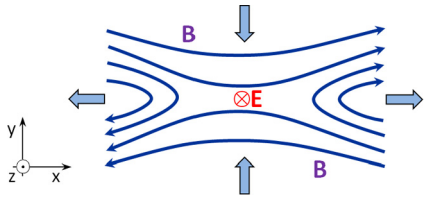


**Fig. 2.** (Colour online.) Sketch of a reconnection region around a X-point. See text for details.

advances. Such mildly relativistic shock waves are possibility encountered in gamma-ray burst outflows (see [47] for a review, as well as [48] in the second volume of this review), in blazar outflows (see, e.g., [49] in the second volume) or trans-relativistic supernovae and they may be the source of cosmic-rays over a wide energy range. Another general question is how the turbulence evolves on much longer timescales than those currently probed by PIC simulations and how does the acceleration of particles to higher energy affect the structure of the shock, e.g., [50].

A strong prediction of Fermi acceleration in the ultra-relativistic limit, as it applies at the external shock of gamma-ray bursts, during their afterglow phase, is the absence of significant polarization, due to the microscopic nature of the turbulence. Another prediction is a reduced maximum synchrotron photon energy, relatively to what might be expected for a Bohm scaling $t_{\rm acc} \sim t_{\rm g}$, due to the fact that the scattering in a micro-turbulence is less efficient than that in a large-scale turbulence (e.g., [51,52]).

### *2.4. Magnetic reconnection*

The process of magnetic reconnection has long been proposed as a source of high-energy particles in the solar corona (e.g., [53] and references therein); in recent years, it has gained popularity as its phenomenological features might explain the rapid variability of blazar flares (e.g., [54]), the flaring high-energy emission of the Crab nebula (e.g., [55,56]) or the pulsed high-energy emission of pulsars (e.g., [57] and references therein). Although the physics of collisionless magnetic reconnection remains largely unexplored, significant advances have been made in the past decade through the use of high performance (HPC) particle-in-cell (PIC) simulations, up to three-dimensional in space.

According to the basic scenario, magnetic reconnection is associated with the dissipation of magnetic energy through non-ideal processes in localized regions. This dissipation transfers energy from the magnetic field to particles and to turbulence. Beyond a simple heating of the plasma, the electromagnetic configuration in the vicinity of reconnection regions allows for efficient particle acceleration. Detailed modern reviews are provided by [58–60].

A generic configuration is that of a X-point, where magnetic field lines incoming from above and below a current sheet meet and annihilate, leading to the formation of a reconnected magnetic field which is advected away to the left and to the right of the reconnection site, see Fig. 2. If the X-point is drawn in the $\boldsymbol{x}$–$\boldsymbol{y}$ plane, with a magnetic field oriented along $+\boldsymbol{x}$ (above the current sheet) or along $-\boldsymbol{x}$ (below the current sheet), the reconnected magnetic field has a strong $\boldsymbol{y}$ component. The pressure gradients lead to a stationary situation in which plasma and magnetic fields are advected towards the reconnection site along $-\boldsymbol{y}$ (resp. $+\boldsymbol{y}$) above the current sheet (resp. below) with some velocity $v_{\rm in}$, then expelled away from the reconnection site along $\pm\boldsymbol{x}$. Accordingly, there exists a motional electric field $\boldsymbol{E}_{\mathbf{rec}} = -\boldsymbol{v}_{\mathbf{in}} \times \boldsymbol{B}$ oriented towards $-\boldsymbol{z}$, both above and beneath the current sheet. A steady state situation also implies $\partial_t \boldsymbol{B} = 0$, hence $\boldsymbol{\nabla} \times \boldsymbol{E}_{\mathbf{rec}} = 0$, hence a $y$-independent $E_{\rm rec}$. This reconnection electric field thus persists in the reconnection region, which is essentially devoid of magnetic field. In this reconnection region, acceleration thus proceeds along the electric field as in a linear accelerator [61,62]. If reconnection proceeds with a guide field, meaning a non-vanishing component of $B_z$, then acceleration still occurs in the reconnection region since $\boldsymbol{E} \cdot \boldsymbol{B} \neq 0$ there.

In the above picture, reconnection is believed to initiate along the current sheet through the so-called tearing instability, which leads to the appearance of multiple reconnection sites, separated by magnetic islands, which forms regions of closed field lines (around $O$-points). Particles trapped in a magnetic island are subject to Fermi-type acceleration whenever the island contracts (e.g., [63]).

Other acceleration processes are possible. In particular, the existence of a motional electric field outside the reconnected region, on both sides of the current sheet, permits Fermi-type acceleration whenever a particle can explore this converging electromagnetic structure [64].

A general feature of reconnection scenarios is the generation of a high-energy power-law tail, with a hard spectral index, i.e. $\mathrm{d}N/\mathrm{d}\gamma \propto \gamma^{-p}$ with $p \sim 1 \to 2$; in such case, a small fraction of the particles carries most of the energy. One important question is the efficiency and the rate through which the initial magnetic energy can be transferred into this power-law spectrum. Particle-in-cell simulations suggest that a significant fraction of the energy can be transferred into those plasma particles that experience reconnection but, given that reconnection sites are limited to a small volume, it is not clear yet what fraction of the total energy in a given volume can be transferred and at what rate. Of course, much also remains to be understood for the basic process controlling reconnection.

Another key question is the reconnection rate $v_{\rm in}/c$, which directly controls the magnitude of $E_{\rm rec}$, which in turn help determine the maximal energy and the acceleration rate; in a relativistic setting, recent PIC simulations suggest $v_{\rm in}/c \sim 0.1$, implying an acceleration timescale $t_{\rm acc} \simeq t_{\rm g}/(v_{\rm rec}/c)$ not far from the Bohm timescale (e.g., [65]).

## 3. Radiation of high-energy photons

The physics of high-energy radiation in astrophysical environments is discussed in great detail in textbooks such as [66]. Here, only the introductive aspects are recalled, then the emphasis is put on modern developments and on the application of these energy losses processes to actual scenarios.

### 3.1. Leptonic processes

Electrons accelerated to high energies can radiate high-energy photons through a variety of quantum electrodynamical processes, but synchrotron radiation and inverse Compton radiation are certainly the most general in astrophysics.

#### 3.1.1. Synchrotron radiation

Synchrotron radiation results from the radiation of the electron as it spirals around a magnetic field line. The standard radiation formula of an accelerated charge, expressed through the Liénard–Wiechert potentials leads, after elaborate calculations, to the expression for the synchrotron power and spectrum, see, e.g., [67,68] as well as [66] for details. The electron loses energy, and therefore radiation energy is produced, at a rate given by

$$\frac{\mathrm{d}E_\mathrm{e}}{\mathrm{d}t} = -\frac{4}{3}\sigma_\mathrm{T} U_\mathrm{B} \gamma_\mathrm{e}^2 \beta_\mathrm{e}^2 c \tag{12}$$

with $\gamma_\mathrm{e} = \left(1-\beta_\mathrm{e}^2\right)^{-1/2}$ the Lorentz factor of the electron, $\sigma_\mathrm{T}$ the Thomson cross-section and $U_\mathrm{B}$ the magnetic energy density.

The resulting single particle spectrum has a complicated shape described by Bessel functions but its main properties can be understood as follows: highly relativistic particles ($\gamma_\mathrm{e} \gg 1$) emit most of their radiation in a cone of opening angle $1/\gamma_\mathrm{e}$ due to relativistic beaming; during the spiralling motion, this cone crosses the line of sight to the observer on a timescale $\sim t_\mathrm{g}/\gamma_\mathrm{e}$ with $t_\mathrm{g} = \gamma_\mathrm{e} mc/(eB)$, but this pulse is seen by the observer with a width $\sim t_\mathrm{g}/\gamma_\mathrm{e}^3$ because the front of the pulse preceeds the rear by a length $(1-\beta_\mathrm{e})ct_\mathrm{g}/\gamma_\mathrm{e}$; therefore the characteristic frequency of synchrotron radiation, where the spectrum peaks is $\nu_\mathrm{syn} \propto \gamma_\mathrm{e}^3/t_\mathrm{g} \simeq 4.3\times 10^6 \gamma_\mathrm{e}^2 B_{-4}$ Hz ($B_{-4} = B/1$ T). Below this frequency, the characteristic spectral energy distribution (SED) $\nu P_\nu$ emitted by a single particle scales with frequency $\nu$ as $\nu P_\nu \propto \nu^{4/3}$, and it cuts off roughly exponentially above. Of course, if the comoving frame is moving towards the observer with a bulk Lorentz factor $\Gamma$, the synchrotron emission is angularly beamed towards the observer, implying an increase of the flux by a factor $\sim\Gamma^2$, while the peak frequency is increased by $\sim\Gamma$.

The synchrotron spectrum of a population of electrons can be obtained by folding the above power with the electron distribution; for a power-law, $\mathrm{d}N_\mathrm{e}/\mathrm{d}\gamma \simeq \gamma^{-p}$, one finds easily $P_\nu \propto \nu^{-(p-1)/2}$: there are $\gamma\,\mathrm{d}N/\mathrm{d}\gamma \propto \gamma^{1-p}$ electrons in a log-interval $\log\gamma$, emitting a power $\propto \gamma^2$ [Eq. (12)]; noting that $\gamma \propto \nu^{1/2}$, one arrives at the above result.

As discussed in Section 2, the maximal (electron) synchrotron photon energy is limited by the competition of the energy gain with the radiation loss to a value of the order of $70\,\mathcal{A}^{-1}$ MeV in the absence of relativistic bulk motion of the source, assuming that the acceleration timescale $t_\mathrm{acc} = \mathcal{A}^{-1} t_\mathrm{g}$ [14]. Therefore, electron synchrotron photons cannot populate the highest energy parts of the spectrum, unless the source moves at a large Lorentz factor towards the observer. In gamma-ray bursts, the synchrotron emission of electrons accelerated at the external ultra-relativistic shocks may nevertheless explain the long-lived GeV emission (e.g., [69], see also [48]). As mentioned previously, however, the maximum synchrotron photon energy in such shock waves remains limited to values of the order of 1 GeV on 100–1000 s timescales, even for bulk Lorentz factors as large as a few hundreds, due to the relatively inefficient scattering properties of the micro-turbulence in the vicinity of the shock (e.g., [51,52]). Consequently, the highest photons, with $\epsilon_\gamma \gtrsim 10$ GeV observed in some bursts, must have been produced through inverse Compton radiation [70], discussed next.

An interesting and original alternative to produce high-energy photons through electron synchrotron radiation is to generate very-high-energy electrons, with $E_\mathrm{e} \gtrsim 10^{17}$ eV, through the pair production of very-high-energy ions on the cosmic microwave background; such electrons can then radiate GeV–TeV photons in extra-galactic magnetic fields, offering a valuable signature of ion acceleration to these extreme energies, e.g., [71].

The standard synchrotron calculation assumes that the electron gyrates around a straight magnetic field line. In a magnetized turbulence, the general features of the radiation spectrum may thus differ somewhat. The deviations are strongest when the particle explores several coherence cells of the turbulence while its emission cone of opening angle $1/\gamma$ remains focused towards the observer; in this case, one speaks of jitter radiation, e.g., [72,73]. Which situation takes place is parameterized by the wiggler parameter

$$a = \frac{e\delta B \lambda_{\delta\mathrm{B}}}{m_\mathrm{e} c^2} \tag{13}$$

If $a \ll 1$, then the particle is deflected by less than $1/\gamma$ while crossing a coherence cell of length $\lambda_{\delta\mathrm{B}}$, therefore the jitter regime applies and alters the spectrum below the peak frequency, with a characteristic dependence $\nu^0$ (instead of $\nu^{1/3}$) for $P_\nu$. If $1 \ll a \ll \gamma$, a moderate jitter regime applies, with modifications of the spectrum at frequencies $\nu < a^{-3}\nu_\mathrm{syn}$ and above $\nu_\mathrm{syn}$. Finally, for $\gamma \ll a$, the standard synchrotron paradigm applies, even in a strong turbulence, because the particle only explores one coherence cell during its emission. Of course, one strong signature of radiation in a micro-turbulence is the absence of net polarization, which may otherwise take values of tens of percent in an ordered magnetic field.

*3.1.2. Inverse Compton radiation*

Inverse Compton radiation is emitted through the upscattering of seed radiation, i.e. $\mathrm{e}^- + \gamma_\mathrm{b} \to \mathrm{e}^- + \gamma$, where $\gamma_\mathrm{b}$ represents here a seed or background photon, while $\gamma$ denotes the upscattered photon. In the Thomson limit, the photon energy in the electron rest frame does not exceeds its rest mass energy, i.e. $\gamma_\mathrm{e}\epsilon_{\gamma_\mathrm{b}}(1-\beta_\mathrm{e}\cos\theta) < m_\mathrm{e}c^2$, with $\gamma_\mathrm{e}$ the Lorentz factor of the electron, $\epsilon_{\gamma_\mathrm{b}}$ the energy of the seed photon and $\theta$ the angle between the momenta of the electron and of the photon. In this Thomson limit $\epsilon_{\gamma_\mathrm{b}} \ll m_\mathrm{e}c^2/\gamma_\mathrm{e}$, the mean energy of the upscattered photon is $\epsilon_\gamma \simeq 2\gamma_\mathrm{e}^2\epsilon_{\gamma_\mathrm{b}}$. The reason for the factor $2\gamma_\mathrm{e}^2$ is actually the same as for a Fermi process: in the rest frame of the electron, the photon suffers angular scattering with little energy change; going to this rest frame and back, after random angular deflection, the photon energy is increased by $2\gamma_\mathrm{e}^2$ on average, through the same kinematic process as in a relativistic shock.

In the Thomson limit, the electron loses energy at a rate

$$\frac{\mathrm{d}E_\mathrm{e}}{\mathrm{d}t} = -\frac{4}{3}\sigma_\mathrm{T}U_\mathrm{rad}\gamma_\mathrm{e}^2\beta_\mathrm{e}^2 c \tag{14}$$

an expression very similar to that for synchrotron losses, expressed here in terms of the radiation energy density $U_\mathrm{rad}$. As a result, it is common practice to treat the inverse Compton losses on the same footing as synchrotron losses, by assigning an equivalent magnetic field strength to the radiation background: for instance, inverse Compton losses on the cosmic microwave background can be described as synchrotron losses in a magnetic field of strength $3.3{\cdot}10^{-10}$ T.

The spectrum emitted by a power-law population of electrons is obtained by folding the electron distribution $f_\mathrm{e}$ over the seed photon distribution $f_\gamma$ and the cross-section. The emissivity reads

$$\frac{\mathrm{d}n_\gamma}{\mathrm{d}t\mathrm{d}^3p_\gamma} = \int \mathrm{d}^3p_{\gamma_\mathrm{b}}\, f_\gamma(\boldsymbol{p}_{\gamma_\mathrm{b}}) \int \mathrm{d}^3p_\mathrm{e}\, f_\mathrm{e}\left(\boldsymbol{p}_\mathrm{e}\right)\, (1-\beta_\mathrm{e}\cos\theta)\, \frac{\mathrm{d}\sigma}{\mathrm{d}^3p_\gamma}c \tag{15}$$

where all quantities are written in the comoving source frame. An additional Lorentz transform on $\mathrm{d}^3p_\gamma$ on the r.h.s. is in general necessary to use the differential cross-section in the electron rest frame.

In the Thomson limit and single Thomson scattering limit, in which one neglects the possibility of rescattering the Compton scattered radiation, a simple approximation for the above writes the differential cross-section as $(4\pi p_\gamma^2)^{-1}\sigma_\mathrm{T}\delta\left(p_\gamma - 2\gamma^2 p_{\gamma_\mathrm{b}}\right)$ and ignores the angular dependence. For an isotropic electron power-law distribution with spectral index $p$ ($p > 2$) in an isotropic photon background strongly peaked at $\epsilon_{\gamma_\mathrm{b}}$, the resulting photon spectrum is a power-law of slope $-(p-1)/2$, as for synchrotron, peaking at $\approx 2\gamma_{\mathrm{e,min}}^2\epsilon_{\gamma_\mathrm{b}}$. Different approximations and/or more general distributions lead to different spectral dependencies. Multiple Compton scattering leads to rather characteristic spectra, with each Compton order separated from the previous one by a factor $2\gamma_{\mathrm{e,min}}^2$, until the Klein–Nishina limit is reached.

This Klein–Nishina limit corresponds to $\epsilon_{\gamma_\mathrm{b}} \gtrsim m_\mathrm{e}c^2/\gamma_\mathrm{e}$, i.e. a photon energy exceeding the rest mass energy $m_\mathrm{e}c^2$ in the electron rest frame. The cross-section decreases roughly as $\log\epsilon_{\gamma_\mathrm{b}}/\epsilon_{\gamma_\mathrm{b}}$ above this threshold and the energy gained by the photon is of course limited to the energy of the electron, i.e. $\epsilon_\gamma \leq \gamma_\mathrm{e}m_\mathrm{e}c^2$. A convenient approximation uses the Thomson formula Eq. (14) but truncates the radiation background energy density at the Klein–Nishina limit, i.e. $U_\mathrm{rad} \to U_\mathrm{rad}\left(\epsilon_{\gamma_\mathrm{b}} < m_\mathrm{e}c^2/\gamma_\mathrm{e}\right)$. For detailed calculations, see [74].

A fundamental application of synchrotron and inverse Compton losses in high-energy astrophysics is the synchrotron self-Compton (SSC) process, through which the high-energy electrons upscatter the synchrotron background that they themselves produce. This process is one essential building block of the standard model of high-energy radiation from relativistic jets in active galactic nuclei and in gamma-ray bursts. The inverse Compton emission is detected nearly routinely in active galactic nuclei, see notably [49] in the second volume of this review, but there exist only a handful potential detections for gamma-ray bursts. Stringent upper limits have been obtained recently on the TeV emission from gamma-ray bursts by VERITAS (GRB130427A [75]) and H.E.S.S. (GRB100621A [76]).

In the SSC scenario, useful relations can be obtained directly from the arguments presented above. In the Thomson limit, assuming here as well single Compton scattering, the ratio of the cooling rates through inverse Compton scattering Eq. (14) and through synchrotron Eq. (12) implies that the ratio of the inverse Compton power $P_\mathrm{IC}$ to synchrotron power $P_\mathrm{syn}$ verifies

$$\frac{P_\mathrm{IC}}{P_\mathrm{syn}} \simeq \frac{U_\mathrm{rad}}{U_\mathrm{B}} \simeq \frac{U_\mathrm{syn}}{U_\mathrm{B}} \tag{16}$$

This ratio corresponds to the Compton parameter $Y \simeq \sigma_\mathrm{T}n_\mathrm{e}r\langle\gamma_\mathrm{e}^2\rangle$, $n_\mathrm{e}$ and $r$ respectively representing the electron density and radius of the emitting region; the average is taken over the electron distribution in the emitting region. This Compton parameter represents the mean energy gain of photons (in units of $m_\mathrm{e}c^2$), weighted by the interaction probability.

Another useful relation is that which ties the peak of the inverse Compton spectrum to that of the synchrotron component: $\nu_{\mathrm{IC,peak}} \simeq 2\langle\gamma_\mathrm{e}^2\rangle\nu_{\mathrm{syn,peak}}$. Of course, any deviation from the Thomson approximation, or multiple Compton scattering, can strongly modify these relationships.

Relativistic aberration can also strongly affect the way an object is perceived by the observer. For an emitting region moving with bulk Lorentz factor $\Gamma$ (velocity $\beta c$) at angle $\theta$ away from the line of sight from the central source to the observer, one defines the Doppler parameter $\mathcal{D} = [\Gamma(1-\beta\cos\theta)]^{-1}$; the angle $\theta$ is defined in the source rest frame.

A comoving frequency $\nu'$ becomes $\nu = \mathcal{D}\nu'$ through Lorentz transform; it is thus boosted by $\Gamma$ if $\theta \lesssim 1/\Gamma$ as mentioned earlier, and otherwise deboosted by $1/\Gamma$. The specific intensity $I_\nu$ of the radiation, which defines the amount of energy transported per unit surface area, per unit solid angle, per unit time and per unit frequency, transforms as $\nu^3$, hence $I_\nu = \mathcal{D}^3 I'_{\nu'}$. Similarly, one can show that the observed spectral flux $F_\nu \propto \mathcal{D}^q L'_{\nu'}$, in terms of the proper spectral luminosity $L'_{\nu'}$ at (observer) frequency $\nu$; $q = 2+\alpha$ for a jet-like emitting region with spectral index $\alpha = -\mathrm{d}\log I'_{\nu'}/\mathrm{d}\log\nu'$, $q = 3+\alpha$ for a blob-like region [77].

For similar reasons, any radiation produced outside the jet can be strongly enhanced in the jet frame and therefore modify the standard SSC paradigm. In blazars, an obvious candidate for such external Compton radiation is the flux emitted by the surrounding accretion disk and torus [78]. In this external Compton scenario, the radiation measured by the observer has a different Doppler dependence, e.g., $F_\nu \propto \mathcal{D}^{4+2\alpha}$, and possibly, a different spectral dependence. This introduces additional freedom in modelling which is needed in certain blazar classes, as discussed in the second volume of this review [49].

#### 3.1.3. Other radiative processes

In specific situations, other processes may be of importance, for instance curvature radiation in a pulsar magnetosphere (e.g., [79] this volume), in which the electron radiates along curved magnetic field lines, or pair cascades, in which the electron upscatters a background photon through inverse Compton losses, which then converts back into an electron (or a positron) through pair production processes etc. The latter is of importance in high-energy astrophysics, because it shapes the high-energy cut-off of extra-galactic sources through absorption in the diffuse extragalactic backgrounds, as discussed in the second volume of this review [80].

### 3.2. Hadronic processes

The two leading hadronic processes which lead to the production of high-energy photons in astrophysical sources are inelastic pp collisions and photo-hadronic pγ interactions. Nuclei are also subject to such interactions, but in many cases, and particularly so at high energies, these processes can be described as the interaction of single nucleons inside the nucleus.

Protons can also lose energy through synchrotron. However, at a same energy, the emitted power is a factor $(m_\mathrm{p}/m_\mathrm{e})^4$ lower than the corresponding energy loss rate for electrons, therefore proton synchrotron radiation only becomes efficient in intense magnetic fields and at high energies. Nevertheless, proton synchrotron radiation can reach energies higher than the electron radiation reaction limit by a factor $m_\mathrm{p}/m_\mathrm{e}$. This process has been invoked in some blazar scenarios to explain the highest energy part of the spectrum, e.g., [81,82].

A common feature of pp and pγ processes is the production of pions, which then decay into photons ($\pi^0 \to \gamma+\gamma$) and neutrinos (e.g., $\pi^+ \to \mu^+ + \nu_\mu$, $\mu^+ \to \mathrm{e}^+ + \nu_\mathrm{e} + \bar{\nu}_\mu$), with the generic prediction of a comparable luminosity between photons and neutrinos in each flavor $L_\gamma \sim L_\nu$. This provides a beautiful connection between cosmic ray, neutrino and high-energy-photon astrophysics [83].

#### 3.2.1. pp Collisions

Photon production in inelastic reactions such as $\mathrm{p}+\mathrm{p} \to \mathrm{p}+\mathrm{p}+\pi+\ldots$ likely explains the high-energy emission from the disk of the Milky way, through the collisions between cosmic ray protons and interstellar gas, see [84] in this volume. Detailed calculations indeed show that the observed flux is in good agreement with the predicted emissivity of the interstellar gas (e.g., [85,86]). This implies notably that the cosmic ray flux, which is measured locally in the Solar vicinity, appears as a good estimator of the average cosmic ray sea in the Galaxy.

Another potential use of pp collisions is to trace the acceleration of cosmic ray protons in young supernova remnants through the interaction of these protons with surrounding molecular gas, see, e.g., [87]. Molecular clouds are ideal targets as their "high" gas density, relative to the average interstellar medium, allows them to be illuminated by the cosmic rays when seen in high energy gamma rays. Two such sources have been detected very recently by the H.E.S.S. experiment [88,89]; see [20] in this volume for further discussion.

In general, the emissivity of interstellar gas is written

$$j_\gamma(\epsilon_\gamma) \simeq 4\pi \int_{\epsilon_\gamma} \mathrm{d}E_\mathrm{p}\, \frac{\mathrm{d}n_\mathrm{p}}{\mathrm{d}E_\mathrm{p}}\, \sigma_\mathrm{pp} n_\mathrm{g} c\, Z \tag{17}$$

in terms of the interstellar gas density $n_g$ and the cosmic ray proton distribution function $\mathrm{d}n_\mathrm{p}/\mathrm{d}E_\mathrm{p}$ cross-section $\sigma_\mathrm{pp} \sim 30$ mb (see [85,86] for detailed parameterizations) and the factor $Z$ is the so-called spectrum weighted moment of the inclusive cross-section, which models the energy dependence of the cross-section, see the above references.

#### 3.2.2. pγ interactions

The photo-hadronic interaction is famous for the Greisen–Zatsepin–Kuzmin cut-off [90,91], which should occur at $E_\mathrm{p} \sim 6\times 10^{19}$ eV due to the photo-hadronic interaction with the cosmic microwave background. The reaction $\mathrm{p}+\gamma \to \mathrm{p}+\pi^0$ indeed becomes kinematically allowed when

$$\epsilon_\gamma E_\mathrm{p} \geq \frac{m_\pi\left(m_\pi + 2m_\mathrm{p}\right)c^4}{2(1-\cos\theta)} \tag{18}$$

depending on $\theta$, the angle between the incoming photon and protons in the laboratory frame. The above can be approximated by $\epsilon_\gamma E_\mathrm{p} \gtrsim 0.2\ \mathrm{GeV}^2$. Integrating over the cosmic microwave background photon distribution, one obtains the effective GZK threshold, where a cut-off has indeed been detected recently by the HiRes experiment [92], then by the Pierre Auger Observatory [93].

The decay of the pion produces two photons, which typically carry 5–10% of the parent proton energy. Correspondingly, the inelasticity of this process is $\Delta E_\mathrm{p}/E_\mathrm{p} \sim 0.1$–$0.2$, leading to a rapid degradation of the proton energy. A common and convenient approximation is to describe the cross section through the $\Delta$ resonance, corresponding to the reaction channel $\mathrm{p}+\gamma \to \Delta^+ \to \mathrm{N}+\pi$, with N a proton or a neutron: at the resonance, meaning $\epsilon'_\gamma = 0.3$ GeV where $\epsilon'_\gamma$ is the energy of the photon in the rest frame of the proton, the cross-section is $\sigma_\Delta \simeq 300$ μb. However, multi-pion production contributes to a substantial fraction of the integrated cross-section; hence, above an additional 0.5 GeV threshold, the cross-section reads $\sigma \simeq 0.2\sigma_\Delta + 80$ μb (e.g., [94]).

Although photo-hadronic high-energy photons have never been identified unambiguously in astrophysical sources, this process is seen as a potentially important signature of proton acceleration to very high energies. High proton energies and luminosities are indeed necessary, given the high threshold and the overall weakness of the cross-section. Photo-hadronic interactions are thus expected in compact sources with intense radiation fields produced e.g., by the synchrotron process of electrons accelerated simultaneously. Examples include the signatures left by photo-hadronic photons at very high energies in the prompt phase of gamma-ray bursts [95,96] and the high-energy emission of blazars, either through the acceleration of protons to high energies in a jet dominated by leptons, or in a (hadronic) model where protons dominate the energy budget, see [49].

## 4. Conclusions

The aim of this article has been to provide a short introduction to the physics of particle acceleration and radiation in astrophysical sources. As discussed in Section 2, acceleration occurs mainly through the motional electric fields associated with the motion of magnetized plasmas, because in the rest frame of those plasmas, electric fields are usually efficiently screened. There exist a host of possible acceleration mechanisms, which differ from one another in how the particle is pushed along the motional electric field and how this motional electric field is generated. Section 2 has put emphasis on the most famous acceleration mechanisms, namely acceleration in turbulent flows, acceleration at collisionless shock waves and acceleration in reconnection flows. In general, one can describe to a satisfactory degree of accuracy the physics of acceleration in the test-particle limit, in which one neglects the influence of the accelerated particles on their environment. However, modern developments have shown that, as these accelerated particles draw a substantial fraction of the injected kinetic and/or magnetic energies, they are able to back-react on the flow structure and therefore modify in way the acceleration process. This non-linear relationship, which generally acts on microphysical scales, is the topic of most modern studies in this field.

In contrast, the microphysics of radiation processes, discussed in Section 3, are well known. What hampers a quick and easy comparison of predictions to the data is rather the construction of a model of the source on macrophysical scales with a realistic description of the radiative and magnetohydrodynamical backgrounds. Such quantities are often imperfectly known, if at all, or difficult to model in fine details. The subsequent articles offer clear examples of this complexity.

Nevertheless, the fast development of our knowledge of the violent Universe demonstrates how successful the general interplay between theory and observations has been. With the advent of new instruments at these high energies (see, e.g., [97] in the second volume of this review), the future indeed looks bright for both theorists and observers in this field.

In past decades, and even more so in recent years, numerical simulations have brought in a new way to address the complex and multi-scale nature of these problems. In the field of acceleration physics, particle-in-cell and magnetohydrodynamical simulations have offered refined descriptions of the environment on the microphysical scales of interest, with a direct access to the non-linear relationship between the supra-thermal particles and the surrounding electromagnetic flow structure. Magneto-hydrodynamical, Monte Carlo and radiative transfer simulations have also offered more accurate modellings of the source and of the spectra determinations. These numerical tools are already inescapable and the ever increasing computing facility obviously offers a bright future to this approach.

## Acknowledgements

This work has been supported by the “Programme National Hautes Énergies” (PNHE) of CNRS and by ANR-14-CE33-0019 MACH Project.

## References

[1] D.J. Thompson, C. R. Phys. 16 (2015) 600–609, in this issue.
[2] M. de Naurois, D. Mazin, C. R. Phys. 16 (2015) 610–627, in this issue.
[3] L.O'C. Drury, Space Sci. Rev. 36 (1983) 57.
[4] R.D. Blandford, D. Eichler, Phys. Rep. 154 (1987) 1.
[5] J. Kirk, in: A.O. Benz, T.J.-L. Courvoisiez (Eds.), Saas-Fee Advanced Course, vol. 24, Springer, New York, 1994.
[6] F. Rieger, V. Bosch-Ramon, P. Duffy, Astrophys. Space Sci. 309 (2007) 119.

[7] A. Achterberg, IAC2008, web resource, 2008.
[8] V. Petrosian, A.M. Bykov, Space Sci. Rev. 134 (2008) 207.
[9] A. Bykov, N. Gehrels, H. Krawczynski, M. Lemoine, G. Pelletier, M. Pohl, Space Sci. Rev. 173 (2012) 309.
[10] M. Hoshino, J. Arons, Phys. Fluids B 3 (1991) 818.
[11] Y.A. Gallant, M. Hoshino, A.B. Langdon, J. Arons, C.E. Max, Astrophys. J. 391 (1992) 73.
[12] M. Hoshino, Astrophys. J. 672 (2008) 940.
[13] A.R. Bell, Mon. Not. R. Astron. Soc. 182 (1978) 147.
[14] P.W. Guilbert, A.C. Fabian, M.J. Rees, Mon. Not. R. Astron. Soc. 205 (1983) 593.
[15] E. Fermi, Phys. Rev. 75 (1949) 1169.
[16] G. Pelletier, Astron. Astrophys. 350 (1999) 705.
[17] W.I. Axford, E. Leer, G. Skadron, in: 15th International Cosmic Ray Conference (ICRC), vol. 2, 1977, p. 273.
[18] G.F. Krimsky, Sov. Phys. Dokl. 23 (1977) 327.
[19] R.D. Blandford, J.P. Ostriker, Astrophys. J. 221 (1978) L29.
[20] J.W. Hewitt, M. Lemoine-Goumard, C. R. Phys. 16 (2015) 674–685, in this issue.
[21] F. De Hoffmann, E. Teller, Phys. Rev. 80 (1950) 92.
[22] D. Caprioli, A. Spitkovsky, Astrophys. J. 783 (2014) 91.
[23] D. Caprioli, A. Spitkovsky, Astrophys. J. 794 (2014) 46.
[24] A.R. Bell, Astropart. Phys. 43 (2013) 56.
[25] H.J. Völk, E.G. Berezhko, L.T. Ksenofontov, Astron. Astrophys. 433 (2005) 229.
[26] J. Skilling, Mon. Not. R. Astron. Soc. 173 (1975) 245.
[27] A.R. Bell, Mon. Not. R. Astron. Soc. 353 (2004) 550.
[28] L.O'C. Drury, S.A.E.G. Falle, Mon. Not. R. Astron. Soc. 223 (1986) 353.
[29] P.-O. Lagage, C. Césarsky, Astron. Astrophys. 125 (1983) 249.
[30] Y. Gallant, A. Achterberg, Mon. Not. R. Astron. Soc. 305 (1999) L6.
[31] A. Achterberg, Y. Gallant, J.G. Kirk, A.W. Guthmann, Mon. Not. R. Astron. Soc. 328 (2001) 393.
[32] M. Lemoine, G. Pelletier, Astrophys. J. 589 (2003) L73.
[33] M.C. Begelman, J.G. Kirk, Astrophys. J. 353 (1990) 66.
[34] M. Lemoine, G. Pelletier, B. Revenu, Astrophys. J. 645 (2006) L129.
[35] J. Niemiec, M. Ostrowski, M. Pohl, Astrophys. J. 650 (2006) 1020.
[36] G. Pelletier, M. Lemoine, A. Marcowith, Mon. Not. R. Astron. Soc. 393 (2009) 587.
[37] M. Lemoine, G. Pelletier, Mon. Not. R. Astron. Soc. 402 (2010) 321.
[38] L. Sironi, A. Spitkovsky, J. Arons, Astrophys. J. 771 (2013) 54.
[39] M.V. Medvedev, A. Loeb, Astrophys. J. 526 (1999) 697.
[40] M. Lemoine, G. Pelletier, L. Gremillet, I. Plotnikov, Mon. Not. R. Astron. Soc. 440 (2014) 1365.
[41] M. Lemoine, G. Pelletier, L. Gremillet, I. Plotnikov, Europhys. Lett. 106 (2014) 55001.
[42] J. Kirk, Y. Lyubarsky, J. Pétri, Astrophys. Space Sci. Libr. 357 (2009) 421.
[43] J. Bednarz, M. Ostrowski, Phys. Rev. Lett. 80 (1998) 3911.
[44] J.G. Kirk, A. Guthmann, Y. Gallant, A. Achterberg, Astrophys. J. 542 (2000) 235.
[45] U. Keshet, E. Waxman, Phys. Rev. Lett. 94 (2005) 111102.
[46] D.C. Ellison, D.C. Warren, A.M. Bykov, Astrophys. J. 776 (2013) 46.
[47] T. Piran, Rev. Mod. Phys. 76 (2005) 1143.
[48] F. Piron, to be published in a forthcoming dossier of C. R. Physique, continuation of the present one (2016).
[49] C. Dermer, B. Giebels, to be published in a forthcoming dossier of C. R. Physique, continuation of the present one (2016).
[50] U. Keshet, B. Katz, A. Spitkovsky, E. Waxman, Astrophys. J. 693 (2009) 127.
[51] J.G. Kirk, B. Reville, Astrophys. J. 710 (2010) 16.
[52] I. Plotnikov, G. Pelletier, M. Lemoine, Mon. Not. R. Astron. Soc. 430 (2013) 1208.
[53] E.R. Priest, T.G. Forbes, Annu. Rev. Astron. Astrophys. 10 (2002) 313.
[54] D. Giannios, D.A. Uzdensky, M.C. Begelman, Mon. Not. R. Astron. Soc. 402 (2010) 1649.
[55] D.A. Uzdensky, B. Cerutti, M.C. Begelman, Astrophys. J. 737 (2011) L40.
[56] B. Cerutti, D.A. Uzdensky, M.C. Begelman, Astrophys. J. 746 (2012) 148.
[57] B. Cerutti, A. Philippov, K. Parfrey, A. Spitkovsky, Mon. Not. R. Astron. Soc. 448 (2015) 606.
[58] M. Hoshino, Y. Lyubarsky, Space Sci. Rev. 173 (2012) 521.
[59] M. Melzani, PhD thesis, École normale supérieure de Lyon, 2014.
[60] D. Kagan, L. Sironi, B. Cerutti, D. Giannios, arXiv:1412.2451, 2014.
[61] S. Zenitani, M. Hoshino, Astrophys. J. 562 (2001) L63.
[62] S. Zenitani, M. Hoshino, Astrophys. J. 670 (2007) 702.
[63] N. Bessho, A. Bhattacharjee, Astrophys. J. 750 (2012) 129.
[64] D. Giannios, Mon. Not. R. Astron. Soc. 408 (2010) L46.
[65] L. Sironi, A. Spitkovsky, Astrophys. J. 783 (2014) L21.
[66] G.B. Rybicki, A.P. Lightman, Radiative Processes in Astrophysics, Wiley, 2004.
[67] V.L. Ginzburg, S.I. Syrovatskii, Annu. Rev. Astron. Astrophys. 3 (1965) 297.
[68] V.L. Ginzburg, S.I. Syrovatskii, Annu. Rev. Astron. Astrophys. 7 (1969) 375.
[69] P. Kumar, R. Barniol-Duran, Mon. Not. R. Astron. Soc. 400 (2009) L75.
[70] X.-Y. Wang, R.-Y. Liu, M. Lemoine, Astrophys. J. 771 (2013) L33.
[71] F.A. Aharonian, Mon. Not. R. Astron. Soc. 332 (2002) 215.
[72] M.V. Medvedev, J.T. Frederiksen, T. Haugbølle, Å. Nordlund, Astrophys. J. 737 (2011) 55.
[73] S.R. Kelner, F.A. Aharonian, D. Khangulyan, Astrophys. J. 774 (2013) 61.
[74] G.R. Blumenthal, R.J. Gould, Rev. Mod. Phys. 42 (1970) 237.
[75] E. Aliu, et al., VERITAS Collaboration, Astrophys. J. 795 (2014) L3.
[76] A. Abramowski, et al., H.E.S.S. Collaboration, Astron. Astrophys. 565 (2014) A16.
[77] K.R. Lind, R.D. Blandford, Astrophys. J. 295 (1985) 358.
[78] C.L. Dermer, R.S. Schlickeiser, Astrophys. J. 416 (1993) 458.
[79] I.A. Grenier, A.K. Harding, C. R. Phys. 16 (2015) 641–660, in this issue.
[80] D. Horns, A. Jacholkowska, to be published in a forthcoming dossier of C. R. Physique, continuation of the present one (2016).

[81] F. Aharonian, New Astron. 5 (2000) 377.
[82] A. Mücke, R. Protheroe, Astropart. Phys. 15 (2001) 121.
[83] E. Waxman, J. Bahcall, Phys. Rev. D 59 (1999) 023002.
[84] M. Su, C. van Eldik, C. R. Phys. 16 (2015) 686–703, in this issue.
[85] E.G. Berezhko, H.J. Völk, Astropart. Phys. 7 (1997) 183.
[86] F. Aharonian, A. Atoyan, Astron. Astrophys. 362 (1999) 937.
[87] F. Aharonian, L.O'C. Drury, H.J. Völk, Astron. Astrophys. 285 (1994) 645.
[88] A. Abramowski, et al., H.E.S.S. Collaboration, Mon. Not. R. Astron. Soc. 446 (2014) 1163.
[89] A. Abramowski, et al., H.E.S.S. Collaboration, Astron. Astrophys. 574 (2015) A100, arXiv:1412.2251.
[90] K. Greisen, Phys. Rev. Lett. 16 (1966) 748.
[91] G.T. Zatsepin, V.A. Kuzmin, Pis'ma Zh. Eksp. Teor. Fiz. 4 (1966) 114, JETP Lett. 4 (1966) 78.
[92] R.U. Abbasi, et al., The HiRes Collaboration, Phys. Rev. Lett. 100 (2008) 101101.
[93] J. Abraham, et al., The Pierre Auger Collaboration, Phys. Rev. Lett. 101 (2008) 061101.
[94] A. Mücke, J.P. Rachen, R. Engel, R.J. Protheroe, T. Stanev, Publ. Astron. Soc. Aust. 15 (1999) 160.
[95] E. Waxman, Lect. Notes Phys. 576 (2001) 122.
[96] K. Asano, S. Inoue, P. Mészáros, Astrophys. J. 699 (2009) 953.
[97] J. Knödlseder, to be published in a forthcoming dossier of C. R. Physique, continuation of the present one (2016).